https://doi.org/10.5194/egusphere-2026-3904
Preprint. Discussion started: 12 August 2026
© Author(s) 2026. CC BY 4.0 License.

Balloon-borne Measurements of Quasi-static Electric Fields at Stratospheric Altitudes from low Latitudes

Kaliappan Jawahar[1], Prasanna Mahavarkar[2], Chellaiah Selvaraj[2], Samireddipalle Sripathi[1], Subramanian Gurubaran[2], Tanneeru Venkateswara Rao[3] and Ashok Priyadarshan Dimri[2]

[1]Equatorial Geophysical Research Laboratory, Indian Institute of Geomagnetism, Tirunelveli 627 011, India
[2]Indian Institute of Geomagnetism, New Panvel, Navi Mumbai 410 218, India
[3]Balloon Facility, Tata Institute of Fundamental Research, Hyderabad 500 062, India

Correspondence to: S. Gurubaran (gurubaran.subramanian@gmail.com)

Abstract. This paper describes the design, deployment and performance of an improved balloon-borne payload, BEENS-2 (Balloon Experiment on the Electrodynamics of Near Space), developed to measure quasi-static horizontal and vertical electric fields in the low-latitude stratosphere. Measuring weak electric fields (few mV/m) at altitudes up to 32 km presents significant challenges due to ultra-high atmospheric impedance (10^{13}–10^{14} Ω) and payload-induced interference. We present a differential electrometer design utilizing the INA116 instrumentation amplifier to achieve the necessary input impedance and common-mode rejection. To address limitations identified in previous flights, the BEENS-2 configuration employed non-conducting glass-reinforced plastic booms and a redundant, eight-probe setup. We used an inverted probe setup for the vertical field measurements to distinguish ambient vertical electric field from hardware-induced DC offsets. Experimental results from a flight conducted on January 17, 2025, from Hyderabad, India, reveal that electromagnetic noise from the orienter motor significantly masked ambient signals while the motor was in operation. However, by analyzing data during periods when the motor power was withdrawn and the payload slowed down (rotation with < 2 RPM), we successfully recovered horizontal fields of 15–25 mV/m and a vertical field of ~200 mV/m. The high-resolution data confirms the effectiveness of the measurement approach for future studies on stratospheric electric fields at low latitudes.

1 Introduction

Accurate detection of low-level signals in electrically noisy environments, whether in a laboratory or in space, necessitates the use of differential measurement techniques. Operational amplifiers (Op Amps) are commonly employed for this purpose, as their high common-mode rejection ratio allows them amplify the difference between two input signals while suppressing common-mode noise. However, standard Op Amps, with typical input impedances of around 10^6 Ω, are inadequate for applications involving ultra-high impedance sources.

The measurement of atmospheric electric fields, particularly at high altitudes, requires specialized instrumentation amplifiers (In-Amps) with significantly higher input impedances to minimize signal loading and distortion. For ground-based atmospheric

https://doi.org/10.5194/egusphere-2026-3904
Preprint. Discussion started: 12 August 2026
© Author(s) 2026. CC BY 4.0 License.

electric field measurements, an In-Amp with an input impedance of 10^{14} to 10^{15} Ω is necessary. This requirement extends to high-altitude balloon-borne measurements up to 40 km, where atmospheric impedance ranges from 10^{13} to 10^{14} Ω (Holzworth, 1981). Above 40 km, the impedance decreases to 10^{12} Ω and then to 10^{11} Ω; consequently, an In-Amp with 10^{12} to 10^{13} Ω is sufficient for sounding rocket-borne instruments. For satellite-borne ionospheric measurements, electrometers often utilize In-Amps with input impedances of ~10^{9} Ω.

The study of stratospheric electrodynamics is important to our understanding of the Global Electric Circuit (GEC), a framework in which the Earth and the ionosphere act as two large conducting plates with a persistent leakage current (Rycroft et al., 2000; Williams, 2009). Early foundational work by Fahleson (1967) and Mozer and Serlin (1969) established the feasibility of balloon-borne electric field measurements, while subsequent research by Bering et al. (1977) and Kelley (1989) detailed the complex interactions between the middle atmosphere and ionospheric electric fields. More recent observations have further correlated stratospheric vertical current density variations with global lightning activity (Holzworth et al., 2005) and identified high-altitude electrical discharges as among the significant GEC components (Pasko et al., 2002). Several of these studies reinforce the utility of balloon platforms for monitoring the drivers and variability of the GEC, providing a context for the findings presented here from the low-latitude region over Hyderabad.

Measuring electric fields at stratospheric altitudes during fairweather conditions, especially at low latitudes, poses significant challenges. The difficulties arise in sensing weak electric fields (few mV/m) while managing the high impedances necessary for both the sensors and the front-end electronics (Holzworth, 1981). Furthermore, double-probe techniques require the rotation of the central payload to isolate the ambient electric field from the potential DC offsets caused by differences in contact potentials between the probes (Holzworth and Bering, 1998). At low latitudes, regional atmospheric phenomena like tropical convection can significantly influence GEC parameters (e.g., Panneerselvam et al., 2007), necessitating localized high-resolution measurements.

An earlier attempt to measure stratospheric electric fields using the double-probe technique was made during the Balloon Experiment on the Electrodynamics of Near Space (BEENS) on the night of December 14, 2013, from Hyderabad (Gurubaran et al., 2017). To address the technical challenges encountered during the first flight, an improved payload configuration was adopted for the second. This article details the instrument deployment on the gondola, the practical difficulties encountered and the solutions implemented for the BEENS-2 experiment, which was conducted on the night of January 17, 2025. The engineering design and structural validation of this multi-material payload have been detailed in a separate report (Mahavarkar et al., 2026). Section 2 elaborates on the instrumentation, Section 3 presents initial experimental results, and Section 4 summarizes the challenges and the prospects for future experiments conducted from low latitudes.

https://doi.org/10.5194/egusphere-2026-3904
Preprint. Discussion started: 12 August 2026
© Author(s) 2026. CC BY 4.0 License.

2 Details of the Experiment

In the previous BEENS experiment conducted on the night of December 14, 2013, a double-probe configuration was utilized. This setup consisted of two pairs of probes (P1-P2 and P3-P4) in the horizontal direction and an additional probe (P5) deployed on an inclined boom above P1. The P5-P1 pair was used for vertical electric field measurements (Gurubaran et al., 2017; Jawahar et al., 2016). Due to launch vehicle constraints, all booms were initially folded and secured by a stepper motor-operated latch before they were deployed using hydraulically damped spring actuators. The gondola, which was a 1 m x 1 m x 1.2 m (height) aluminium frame supporting the payload electronics, rotated at ~6 RPM. Its orientation, along with that of the deployed booms, was determined by an onboard 3-axis fluxgate magnetometer.

During the measurement phase of BEENS-1, the vertical electric field (Ez) was found to be significantly influenced by the horizontal electric field (Ex) and vice versa. The primary source of nose in these probes was the use of a motor to rotate the gondola, a possibility that arose due to the close proximity of the vertical probe to the motor assembly. Furthermore, this cross-contamination occurred because the signal from the vertical probe (P5) was referenced to that of one of the horizontal probes (P1), leading to mutual interference between the Ex and Ez measurements.

In the redesigned BEENS-2 setup, the gondola was a 0.5 m x 0.5 m x 2 m rectangular frame, featuring two 50-cm spacers (top and bottom) and a central 1-m high payload bay. Within the payload bay, the top deck housed a 3-axis fluxgate magnetometer (FGM) (LEMI-011) and a 4-channel differential electrometer module. Below this, several components were placed: two 4-channel isolation amplifier modules, two power supply modules and a Raspberry Pi-based 8-channel 16-bit data acquisition system. The motor controller for the reaction wheel along with its battery and a Honeywell HMC2003 three-axis magneto-resistive magnetometer (MRM) module (used for redundancy) were housed in the spacer above the top deck. The bottom deck of the payload bay held necessary housekeeping equipment, such as the telemetry/telecommand unit and short-range transceivers (tone transmitters). Finally, the spacer below the bottom deck supported a ballast canister, crucial for maintaining the float altitude of the balloon during its flight.

The choice of the deployable booms appeared to be critical in BEENS-1. Approximately 50% of the 3.5-m boom was constructed from an aluminum U-channel, with the remainder consisting of a glass reinforced plastic (GFRP) rod. An inclined boom was also used; however, its metallic properties introduced noise into the vertical electric field measurements, despite all boom elements being wound with Kapton tape for insulation.

For BEENS-2, we utilized a single 5-m stiff GFRP rod, with an effective probe-to-probe separation of 4.8 m, running across the gondola. Spherical probes of 0.2 m dia (referred to as the x-pair) were mounted at both ends of this rod as shown in Fig. 1a. A second, similar rod was arranged in a crisscross manner to achieve mutually orthogonal positions for the other probe pair (referred as y-pair of probes) in the horizontal plane. A similar crossed pair of booms was provided at the bottom deck.

https://doi.org/10.5194/egusphere-2026-3904
Preprint. Discussion started: 12 August 2026
© Author(s) 2026. CC BY 4.0 License.

This configuration placed the bottom x- and y-pairs of probes face-centred at the bottom of the payload bay, aligned with the x- and y-directions of the 3-axis fluxgate magnetometer. In contrast, the top x- and y-pairs were corner-mounted and aligned with the respective axes of the MRM, with an approximate 45° offset between the top and bottom pairs, as illustrated in Fig. 1(b). Practical limitations prevented an exact vertical alignment or a 90° offset between the top and bottom pairs. Consequently, the BEENS-2 configuration comprised a total of eight probes, compared to five in BEENS-1. Stress bars were added to each boom to minimize mechanical stress and prevent deformation. Figure 2 shows the gondola with the electric field probes mounted at the ends of the extended booms seen ready for launch.

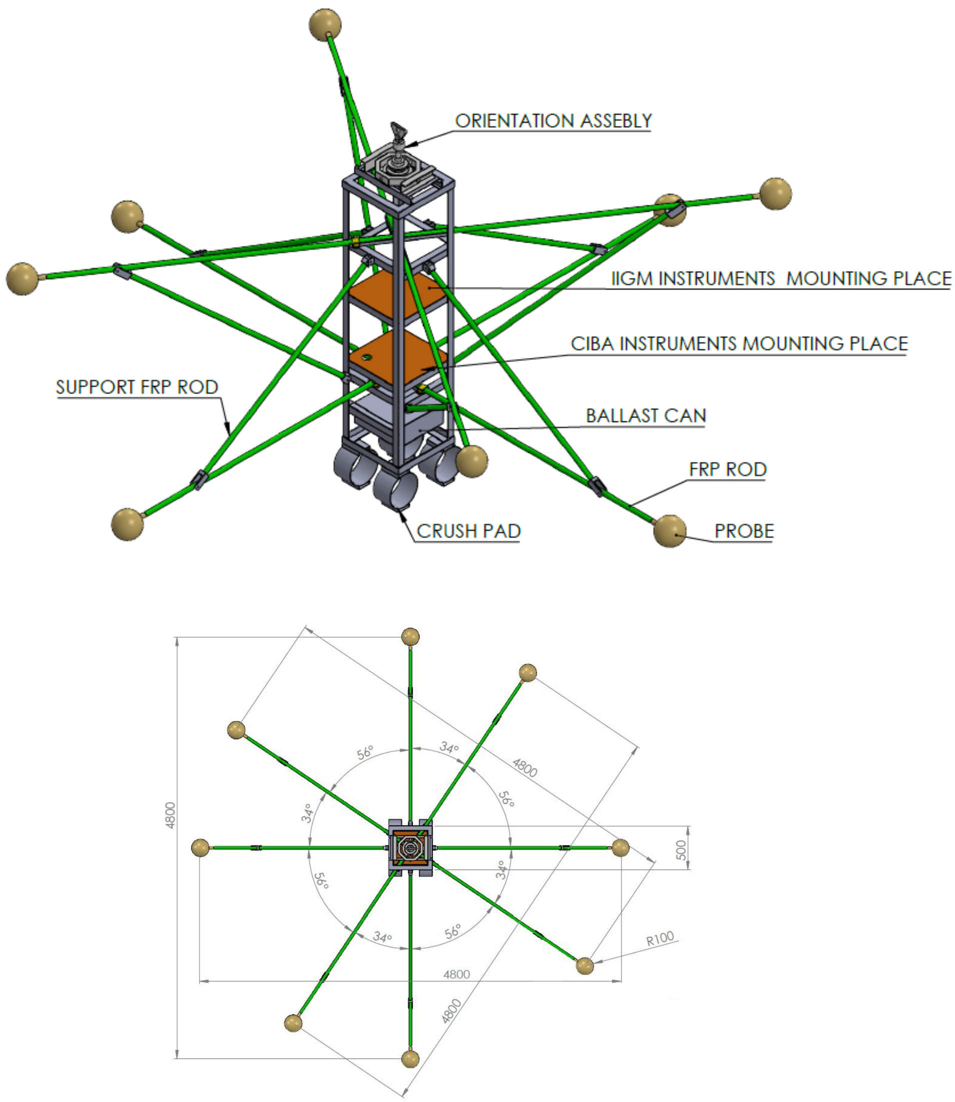

Figure 1: Schematic of the gondola showing the extended boom configuration (top) and the angular separation and relative orientation of the top and bottom probe pairs (bottom).

https://doi.org/10.5194/egusphere-2026-3904
Preprint. Discussion started: 12 August 2026
© Author(s) 2026. CC BY 4.0 License.

Figure 2: The BEENS-2 payload showing the gondola equipped with four pairs of electric field probes. This picture was captured just prior to launch.

The horizontal electric field was estimated from the top and bottom x-pairs of probes (channels 1 and 2), while the vertical electric field was estimated from the top and bottom y-pairs (channels 3 and 4). Moreover, channels 3 and 4 would have opposite polarities, as the measuring cables from the top and bottom probes that form either of the y-pairs were connected to opposite inputs (inverting for one pair and non-inverting for the other) of the electrometer. Not only this arrangement would serve the purpose of redundancy but would also enable verification of the polarity of the measured vertical electric field.

An INA116 In-amp was used in the BEENS-2 differential electrometer. The advantages of this integrated circuit have been detailed elsewhere (Jawahar et al., 2016). RG188 coaxial cables were routed along the booms to connect the probes to the electrometer within the payload bay. Both the booms and cables were wrapped in Kapton tape for insulation. The spherical probes were coated with conductive carbon (Aquadag) to minimize work function differences and suppress photoelectric emission.

https://doi.org/10.5194/egusphere-2026-3904
Preprint. Discussion started: 12 August 2026
© Author(s) 2026. CC BY 4.0 License.

As with BEENS-1, the BEENS-2 payload was designed to spin using a reaction wheel, but at a reduced RPM (2-3 RPM was the target during the design phase) to minimize sine-wave distortion arising from the finite response time (RC constant) of the high-impedance electrometer and its interaction with the ambient environment. The rotation of the gondola induced sinusoidal variations between the top and bottom x-pairs, ~315 degrees out of phase due to the ~45° horizontal offset between the probe pairs. While the signal amplitudes from the top and bottom pairs differed slightly, their temporal variations were identical. These differences in DC offsets were attributed to contact potential differences between the probes and the plasma, any boom misalignment and combined IC offsets within the electrometer.

The vertical electric field was determined from the potential differences between the top and bottom y-pairs of probes. These potential differences manifested as DC voltages of equal magnitude, the average of which represents the vertical electric field. Residual DC offsets, as in the case of horizontal probes, are expected and must be accounted for in the final vertical electric field estimation.

Figure 3: Payload release from the launch vehicle. The gondola and extended booms are visible at the top left, while the balloon itself is outside the frame.

3 Experimental Results

The BEENS-2 was launched from Hyderabad at 22:54 hrs. Indian Standard Time (IST) (= UT + 5.5 hours) on January 17, 2025. A GPS receiver mounted on the load line tracked its flight path. Reaching a float altitude of ~32 km at 00:47 IST, the balloon initially drifted northeast. Later, it drifted westward and maintained a steady westward course until its flight termination at ~06:00 IST the following morning. The payload was successfully recovered after descent. Figure 3 captures the moment of

https://doi.org/10.5194/egusphere-2026-3904
Preprint. Discussion started: 12 August 2026
© Author(s) 2026. CC BY 4.0 License.

payload release from the launch vehicle (balloon is not visible in this picture). Figure 4 illustrates the balloon altitude along with wind speed and direction.

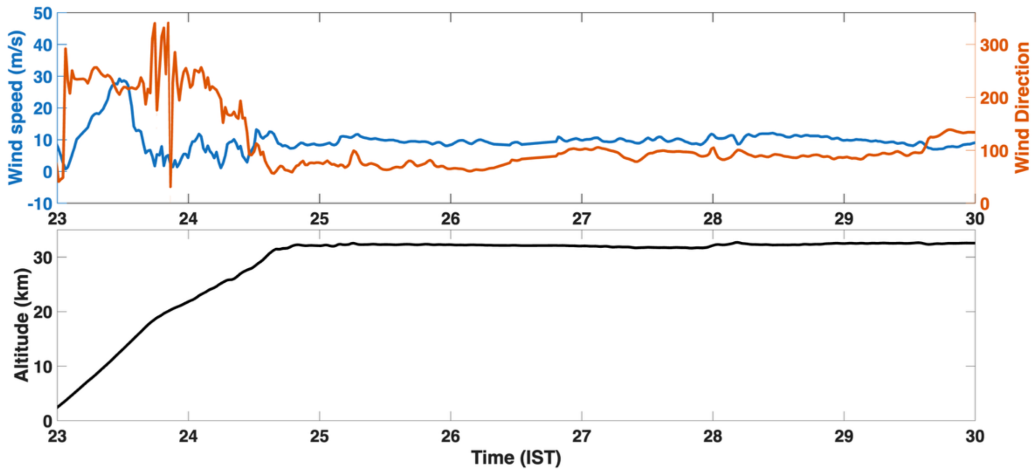

Figure 4: Flight parameters for BEENS-2: wind speed and direction (top panel) and balloon altitude (bottom panel).

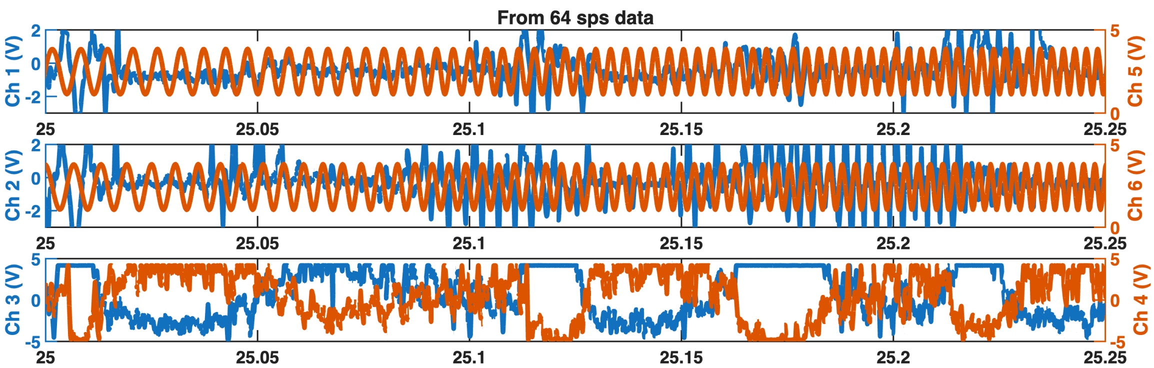

Figure 5: A 15-minute sample (01:00-01:15 IST) illustrating the motor-induced noise in the electric field channels (1 to 4), with the magnetic field channels (5 and 6) revealing no noise. The sinusoidal wave forms in the magnetic field channels with decreasing period reveal an increasing gondola rotation rate in this time segment.

3.1 Analysis of motor-active and motor-inactive durations

Figure 5 presents a 15-minute data sample (01:00-01:15 IST) from the four electric field channels (Channels 1-4, blue) and two magnetic field channels from the fluxgate magnetometer (Channels 5 and 6, red). At this time, the balloon had already reached float altitude. A gain of 10 was applied to the electrometer circuit for channels 1 and 2 via telecommand and so the voltages for these channels shown in Fig. 5 and elsewhere must be divided by 10 for accurate representation. The onboard 16-bit data acquisition system provided a sampling rate of 64 Hz, which was used for the analysis presented here. For the

https://doi.org/10.5194/egusphere-2026-3904
Preprint. Discussion started: 12 August 2026
© Author(s) 2026. CC BY 4.0 License.

magnetometer data comparison, we utilized Channels 5-7 (representing the FGM), since 64 Hz data were only available for the FGM and not the MRM whose data were obtained from the low-resolution telemetry at lower sampling rate.

The sinusoidal waveforms observed in the magnetic field channels confirm the gondola rotation. However, the rotation period varied from ~22 seconds (2.7 RPM) at 01:02 IST (25.001 on the time axis in Fig. 5) to ~10 seconds (6 RPM) at 01:15 IST (25.25), indicating non-uniform rotation. It may be noted that the target uniform rotation of 2-3 RPM could not be achieved during this flight. While the electric field channels are predominantly noisy during this time segment, the horizontal channels (Channel 1: bottom probe pair; Channel 2; top probe pair) show a tendency to follow magnetic field variations. In contrast, the vertical channels (Channels 3 and 4) behave differently. As expected, these two channels exhibit opposite polarities, though one channel experienced more frequent saturation than the other.

The distorted electrical environment and the faster gondola rotation than desired led to the decision to disable the motor via telecommand. Subsequently, the motor was powered only intermittently, specifically, whenever the gondola rotation slowed to 1 RPM or less. This operational strategy resulted in distinct data collection episodes: an 'active mode' where the motor was powered, and a 'passive mode' where the motor was disabled (power to motor withdrawn) and the gondola rotated solely due to its inertia. A significant reduction in noise was observed in the electric field channels during passive mode, yielding clear sinusoidal waveforms, particularly at rotation rates of 1-2 RPM. Minor distortions remained though, likely due to the non-zero charging and discharging times of the probes.

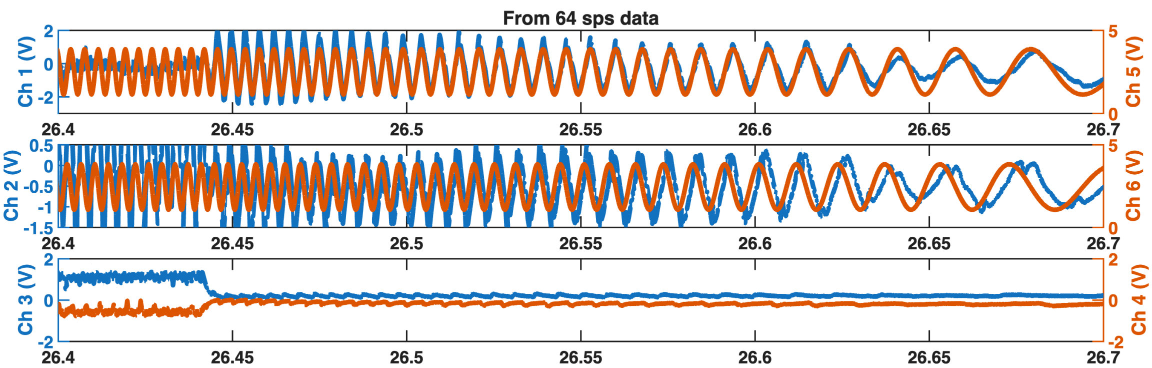

Figure 6: A 15-min data sample (02:27-02:42 IST) during passive mode operation. The increasing period of the sinusoidal waveforms in this time segment indicates a decreasing gondola rotation rate over time. See text for further details.

Figure 6 presents another 15-min data sample (02:27 – 02:42 IST (26.4-26.7)) recorded during a passive mode duration. Over this time segment, the rotation period rose from ~14 s (4.3 RPM) to ~60 s (1 RPM). The electric field channels show systematic variations: near-sinusoidal waveforms in the horizontal channels and nearly steady values but of opposite polarity in the vertical channels. The phase shift between Channel 2 (top probe pair) and Channel 6 (FGM) seen in the middle panel of Fig. 6 is due

https://doi.org/10.5194/egusphere-2026-3904
Preprint. Discussion started: 12 August 2026
© Author(s) 2026. CC BY 4.0 License.

to the geometrical offset between the top and bottom probe pairs and their respective magnetometers (MRM aligned to top probe pair and FGM aligned to bottom probe pair).

Figure 6 also shows a noticeable jump in the vertical electric field channel outputs (Channels 3 and 4) immediately after the motor was powered off. These channels tend to stabilize at ~±200 mV. Figure 7 provides an additional example, clearly illustrating these features during a 6-minute interval (01:51-01:57 IST (25.85-25.95)) when the gondola was rotating in passive mode.

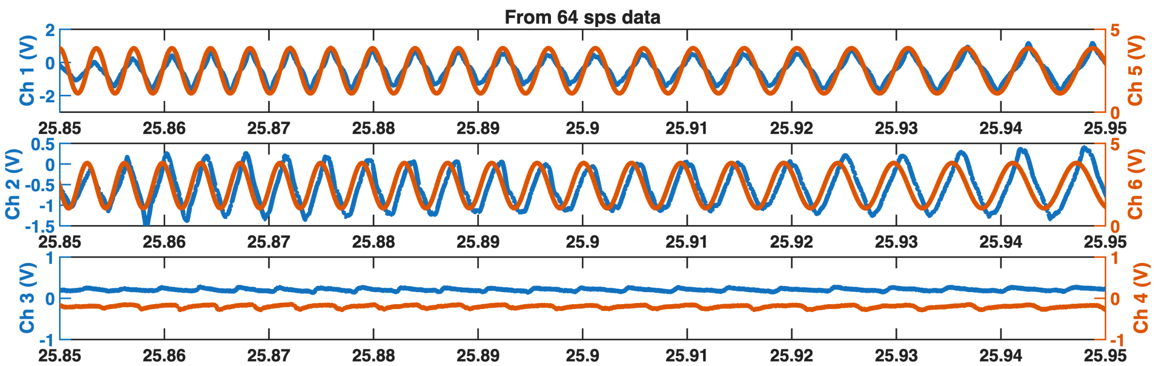

Figure 7: A 6-min data sample during passive rotation, showing clear sinusoidal waveforms in the high resolution (64 Hz) electric field data.

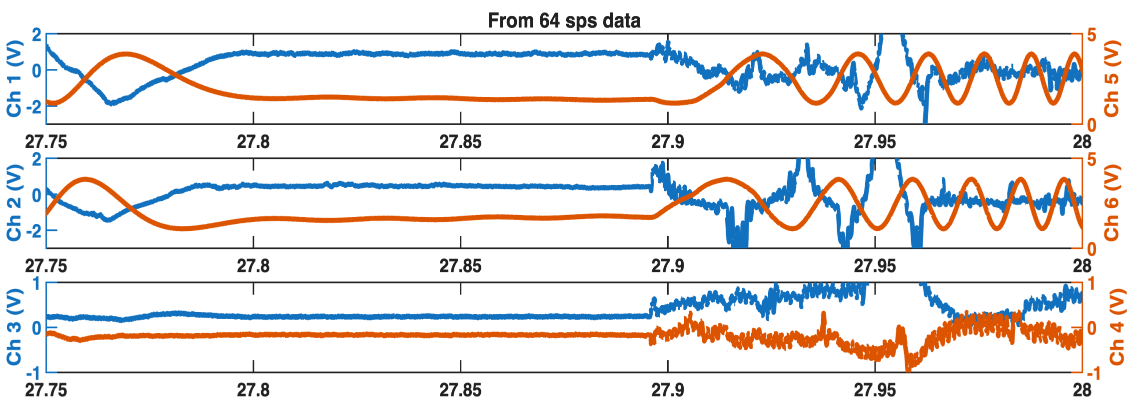

Figure 8: A 15-minute data segment including a 6-min interval when the gondola was non-rotating. See text for details.

Finally, Figure 8 depicts data from the electric and magnetic field channels during the 03:45-04:00 IST (25.85-25.95) segment. During the first half of this interval, the gondola had come to rest, and the motor was reactivated ~6 min later. Throughout this non-rotating period, all channels displayed nearly constant values. This episode serves as a valuable reference for the electric field estimations discussed later.

https://doi.org/10.5194/egusphere-2026-3904
Preprint. Discussion started: 12 August 2026
© Author(s) 2026. CC BY 4.0 License.

Several factors must be considered when estimating and interpreting the electric field components from the BEENS-2 measurements. First, the slight axial offset between the top and bottom pairs of probes directly manifests as a phase difference in the horizontal electric field waveforms. Second, the electromagnetic noise generated during active motor operation significantly overshadowed the ambient electric field signals. Consequently, only the passive mode intervals (when the motor was unpowered) from the nearly five hours of float duration were used for further analysis. The onboard Raspberry Pi-based data acquisition system, featuring a 16-bit ADC, proved superior to the real-time telemetered data retrived using a 12-bit ADC. The telemetry data frequently exhibited signal saturation and clipping, and its lower resolution was insufficient for capturing low-level signals (in the sub-mV range). Furthermore, the onboard system provided a higher temporal resolution (~64 Hz) compared to the telemetry data (~26 Hz). For these reasons, the subsequent analysis is restricted to the data recorded by the dedicated onboard data acquisition system.

3.2 Waveform characteristics and observational features

A brief description of the waveforms observed in the electric and magnetic field channels is necessary before presenting the key observational features. Within the framework of the GEC, horizontal and vertical electric field components originate from different sources (Gupta, 1983), and consequently, they are expected to have different amplitudes when observed at stratospheric altitudes.

Focusing on the horizontal component, it may be recalled that two probe pairs were aligned with the FGM axes (e.g., the x-axis), with the top pair slightly offset relative to the bottom pair. As the gondola rotates, the electric and magnetic field sensors sweep through the ambient field. A highly directional field would produce a sinusoidal waveform during each rotation. For the magnetic field, a maximum value is recorded when the sensor points north, while a minimum is registered when it points south. This directional characteristic is also expected in the two horizontal electric field channels, provided an observable ambient horizontal electric field with a strong directional preference exists. The timing of the electric field maxima and minima depends on the orientation of the ambient field. The variations shown in Figs. 6 and 7 illustrate clear sinusoidal waveforms in electric field channels 1 and 2, along with their magnetic field counterparts (channels 5 and 6).

3.3 Estimation of the horizontal electric field

As previously noted, only the passive mode intervals (motor powered off) are analyzed here. Each of these eight episodes lasted between 10 and 20 min. Due to the larger than desired rotation rates observed at times, power to the orienter motor was withdrawn via ground command, allowing the gondola to decelerate. The motor was reactivated only when the rotation rate dropped below 1 RPM. This cycle was repeated throughout the ~5-hour float duration, yielding eight distinct periods of inertial rotation with significantly reduced noise levels suitable for ambient electric field estimation.

Since the rotation period of the gondola changed continuously during these passive intervals, the waveform amplitude was estimated using the least-squares fitting method for each individual rotation identified from the sinusoidal waveform retrieved from the magnetic field data. In this analysis, the DC offset is treated as one of the fit coefficients. The phase estimated through this least-squares approach directly relates to the orientation of the horizontal electric field component relative to the northward magnetic field component.

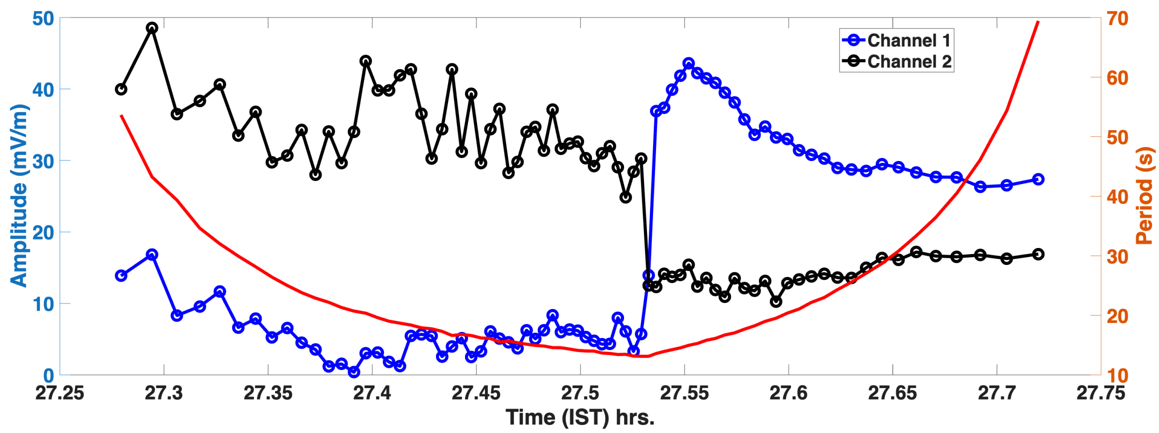

Figure 9: A 25-min data sample (03:17-03:43 IST) showing the stabilization of electric field estimates in Channels 1 and 2 following motor power withdrawal at 03:32 IST (27.53).

3.4 Peculiarities in the observations during motor off periods

It was anticipated that withdrawing motor power would immediately restore the electrical environment for 'clean' measurements. However, observations revealed that it took at least a few minutes for the values to stabilize. Figure 9 illustrates this behavior over a 25-min duration (03:17 – 03:43 IST). At 03:32 IST, the motor power was withdrawn, causing the rotation period to increase from ~15 s to ~70 s by 03:43 IST. Prior to power withdrawal, the estimated electric field values fluctuated, with Channel 2 (black) showing higher values than Channel 1 (blue). Switching off the motor caused sudden jumps in both channels, with Channel 1 subsequently registering higher values than Channel 2. Both channels eventually stabilized by 03:49 IST (~30 mV/m for Channel 1 and ~20 mV/m for Channel 2). Interestingly, Channel 1 experienced a gradual decay after the initial jump, while Channel 2 did not show this behaviour. This sudden jump and subsequent decay in Channel 1 were observed in nearly all eight passive episodes.

Figure 10 consolidates these episodes, with time t=0 defined as the moment when the motor power was withdrawn. Data collected after 05:30 IST were excluded to minimize interference from dawn conditions. The decay in Channel 1 amplitude suggests that the distorted electric field, induced by the operation of the motor, dissipates through the input capacitance of the electrometer as determined by the RC time constant. This decay is clearly evident during the passive rotation periods following

https://doi.org/10.5194/egusphere-2026-3904
Preprint. Discussion started: 12 August 2026
© Author(s) 2026. CC BY 4.0 License.

withdrawal of motor power. Consequently, only estimates corresponding to rotation periods of 30 s or longer (≤ 2 RPM) are considered representative of the undisturbed ambient electric field.

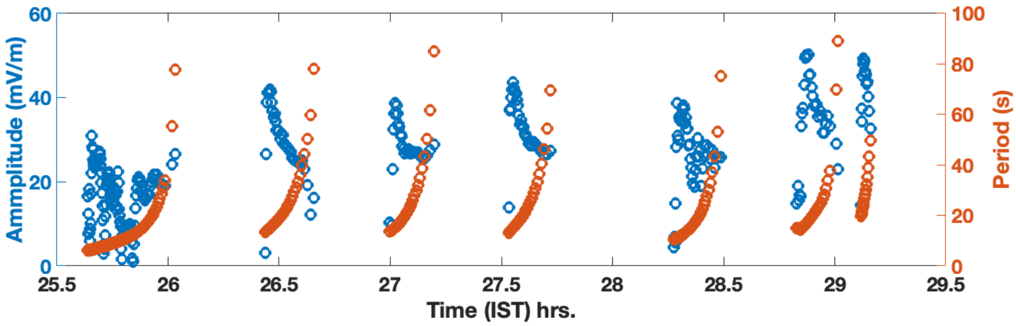

Figure 10: Horizontal electric field estimates (blue) from Channel 1 and rotation period (red) for all passive episodes (excluding dawn conditions).

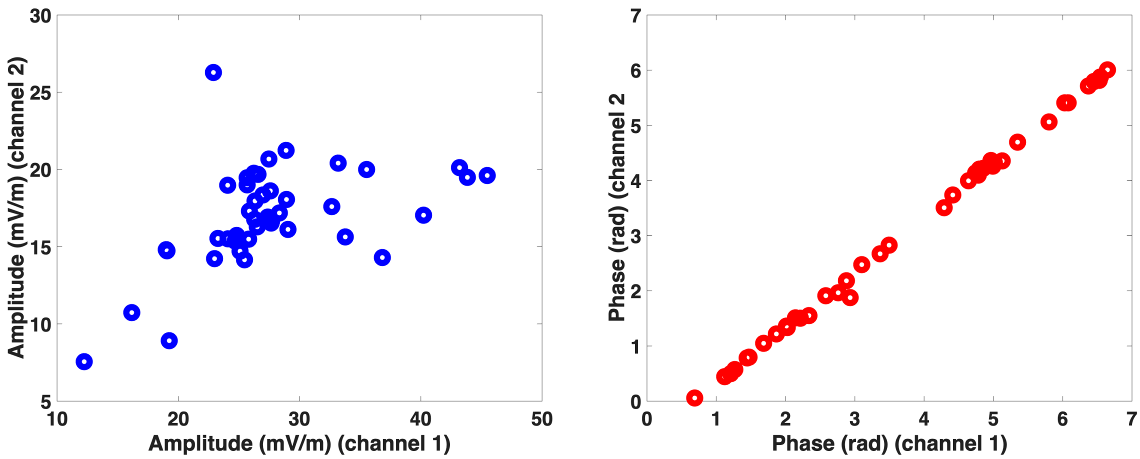

Figure 11: Comparison of horizontal electric electric field amplitude (left) and phase (right) between the top (Channel 2) and bottom (Channel 1) probe pairs during passive rotation (≤ 2 RPM).

Figure 11 compares horizontal electric field estimates for the two channels (1 and 2), with the left panel showing amplitude and the right panel showing phase. This analysis considers only passive rotation periods with rates of 2 RPM or less, spanning over three hours (01:59 to 05:10 IST) at a float altitude of ~32 km. While the estimates for the top probe pair (Channel 2) are 5-10 mV/m lower than those for the bottom probe pair (Channel 1) and exhibit considerable scatter, the phases are remarkably consistent. The constant phase difference between the two channels as seen in the right panel of Fig. 11 reflects the geometrical offset between the top and bottom probe pairs, both referenced to the FGM for the analysis. The strong phase agreement across the 0 to 2π range confirms that both probe pairs sensed the same horizontal electric field these during passive rotation intervals. While the reduced amplitude in Channel 2 was likely due to its proximity to the reaction wheel assembly and orienter motor, the individual horizontal measurements remain unaffected by the vertical electric field because of their differential nature. It is important to note that while the central gondola was surrounded by grounded aluminium plates (coated with Aquadag) to

https://doi.org/10.5194/egusphere-2026-3904
Preprint. Discussion started: 12 August 2026
© Author(s) 2026. CC BY 4.0 License.

provide a stable reference for these differential measurements, the reaction wheel and motor assembly were electrically floating. The proximity of this floating conducting mass to the top probe pair likely introduced a local shielding effect and field line distortion that was not present for the bottom pair. This electrical asymmetry explains why the top pair registered lower amplitudes than the bottom pair, despite both being deployed at the same ~2.5 m distance from the central gondola frame. Interestingly, the amplitude scaling between the two channels appears to shift over time, with Channel 1 registering relatively higher amplitudes during the early dawn hours.

3.4 Estimates of vertical electric field from channels 3 and 4

Several factors must be considered when estimating the vertical electric field. While the top and bottom of x-probes (aligned horizontally) were used for horizontal electric field measurements, the top and bottom pairs of y-probes were utilized for the vertical electric field measurements. These y-probes were aligned with respect to a vertical axis with a 1-m separation between the top and bottom sensors (see Figs. 1 and 2). Although this setup provided redundancy, their connections to the non-inverting (+) and inverting (-) inputs of the electrometer were intentionally reversed prior to launch. As a result, we expected measured voltages with opposite polarity from channels 3 and 4, a featured confirmed by the data shown in Figs. 5 through 8.

Within the context of the GEC, global thunderstorm activity serves as a primary quasi-DC source of the large potential difference prevailing between the Earth and the ionosphere. These act as two large conducting plates with a small leakage current (Hays and Roble, 1979). Near the surface, a potential difference of ~100 V/m exists, which decreases with altitude as atmospheric conductivity increases. At stratospheric altitudes, vertical electric fields typically range from 0.1 to 1 V/m (Holzworth, 1981; Udare et al., 1991).

Estimating the electric field using the double probe technique depends on the uniformity of the probe surfaces and the mitigation of leakage currents from instrumentation amplifiers and circuit boards. For a payload rotating about its vertical axis, these unknowns manifest as a DC offset. While rotation allows for the easy deduction of the horizontal electric field by eliminating this offset, directly estimating the vertical field is more complex because the DC offsets add to or subtract from the ambient field.

In this experimental setup, we obtained two independent sets of horizontal and two independent sets of vertical electric field measurements. By reversing the input connections for the vertical probe pairs, one pair measure (V_z + $(\text{offset})_1$) and the other measure ($-V_z$ – $(\text{offset})_2$). The horizontal probe offsets were determined to be 0.03 V (bottom) and 0.045 V (top). However, the vertical offsets cannot be determined directly. Nevertheless, the two independent measurements allow for a simple method to estimate the potential gradient, namely, take the difference between the two measurements and then divide by two (V_z = (V_z^{EBT}-V_z^{WTB})/2). Here, V_z^{EBT} is the voltage from the east side bottom-top pair of y-probes and V_z^{WTB} is the potential difference from the west side top-bottom pair, where 'east' and 'west' refer to the y-axis directions orthogonal to the north-south (x-axis)

https://doi.org/10.5194/egusphere-2026-3904
Preprint. Discussion started: 12 August 2026
© Author(s) 2026. CC BY 4.0 License.

orientation of FGM. The resulting vertical electric field is estimated to be ~200 mV/m (as detailed below) and is also evident in Figs. 6 to 8 (bottom panels) as the measured potential differences between the probe pairs, with the separation distance between the vertical probes being 1 m.

Given the substantial vertical electric field observed, any residual uncertainty or difference in DC offsets between the two probe pairs is expected to contribute a maximum error of 10% to the final value. This 'reversed connection' approach effectively introduces a spatial reversal, providing a robust means to distinguish the quasi-DC vertical field from hardware-induced biases. The consistent mirror-image polarities observed in the data (Channels 3 and 4) further confirm this approach, demonstrating that common-mode systematic errors are significantly minimized.

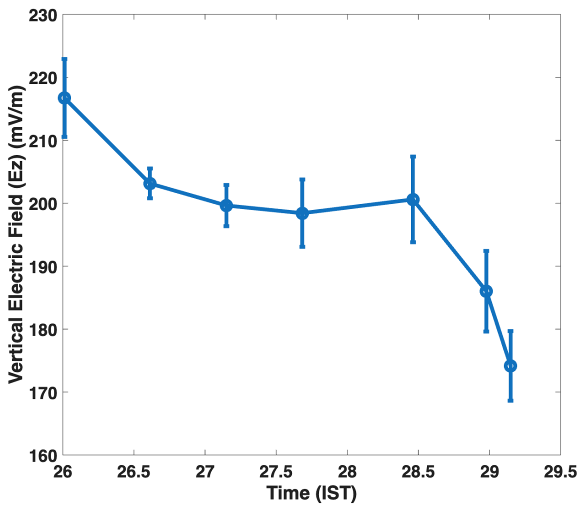

Figure 12: Derived vertical electric field (E_z) during passive rotation intervals (≤ 2 RPM) at float altitude (~32 km). The E_z values were calculated by taking the half-difference of the potential differences measured by the two independent vertical probe pairs (Channels 3 and 4). The error bars represent the standard deviation of individual estimates within a passive rotation interval.

As with the horizontal field, only passive mode intervals are considered for the estimation of vertical electric field, as during periods of active motor operation, the vertical channels exhibited significant noise and fluctuations (see Fig. 5). Figure 12 presents the variation of the derived vertical electric field (E_z) with time calculated using the half-difference method for the passive rotation periods (≤ 2 RPM) at float altitude. The stability of the estimated values at ~200 mV/m during these quiet intervals confirms that the motor-induced interference was the primary source of degradation of the probe outputs and the consideration of only passive mode intervals enabled successful recovery of the undisturbed ambient vertical electric field.

The vertical electric field values obtained in this work are consistent with an earlier report by Udare et al. (1991). This work presented results from two balloon flights from Hyderabad on 8 April 1987 and 6 December 1989. Using two spatially separated wire antennas, the measurements revealed a value of Ez of ~200 mV/m at an altitude of 32 km. The close agreement

https://doi.org/10.5194/egusphere-2026-3904
Preprint. Discussion started: 12 August 2026
© Author(s) 2026. CC BY 4.0 License.

between our results and these earlier findings from the same site further validates the reliability of the double probe configuration and the polar-reversal technique leading to offset cancellation employed in the BEENS-2 experiment.

4. Discussion and Summary

The BEENS-2 experiment successfully demonstrated an improved methodology for measuring stratospheric electric fields at low latitudes. By utilizing non-conducting GFRP booms and a redundant, polarity-reversed probe configuration, we addressed the hardware-induced limitations identified in BEENS-1, ensuring the recovery of useful horizontal and vertical electric field measurements. In BEENS-2, the necessity of a 'passive' rotation mode turned out to be a blessing in disguise. Since controlled motor operation at a steady 2 RPM rotation was not possible, intermittent power cycles were required to sustain gondola rotation. We observed that electromagnetic interference from the orienter motor during active rotation significantly overshadowed the low-level ambient signals. Upon withdrawing motor power, the measurements required several minutes to stabilize as the probes discharged through the electrometer input capacitance, a process that reached completion as the gondola rotation slowed to below 2 RPM. This strategy of intermittent power withdrawal enabled noise-free measurements during inertial rotation, revealing that rotation rates below 2 RPM in the absence of motor-induced noise are optimal for high sensitivity stratospheric electric field measurements.

The horizontal electric field values estimated during the passive episodes (1-2 RPM) were in the range of 15-25 mV/m. These values are notably larger than the 5-10 mV/m reported from the BEENS-1 experiment (Jawahar et al., 2016). As there was no major geomagnetic storm occurring during the flight, the causative mechanisms under investigation emphasize the potential role of mesoscale atmospheric gravity waves in generating these noticeable electric fields at low latitudes. These observations are in line with the findings from the ELBBO experiment, which confirmed a new source of stratospheric horizontal electric fields first reported in 1989 with wide latitude coverage (Holzworth and Bering, 1998). This newly identified field was reported to have an average magnitude of 10 to 20 mV/m at night and 100 to 150 mV/m during the daytime. Its field vector revealed a unique counterclockwise rotation in the southern hemisphere, with a rotation period near the atmospheric inertial wave period. The horizontal scale size of this field was ~500 km, corresponding to the horizontal wavelength of stratospheric inertial waves. This field appears to be a steady background feature of the stratosphere, subject to local disturbances from underlying thunderstorms or other sources.

The scientific results for the vertical component of the electric field are equally encouraging. The vertical electric field estimate of ~200 mV/m at 32 km altitude shows excellent agreement with an earlier report from the same site by Udare et al. (1991). This consistency across decades underscores the stability of the GEC parameters over the Hyderabad region. Furthermore, the strong phase agreement between the top and bottom horizontal probe pairs, despite the amplitude reduction observed in the top pair, confirms that the directional information of the retrieved stratospheric field is highly reliable. The observed amplitude

https://doi.org/10.5194/egusphere-2026-3904
Preprint. Discussion started: 12 August 2026
© Author(s) 2026. CC BY 4.0 License.

reduction in Channel 2 highlights the importance of local shielding effects. The proximity of the reaction wheel and motor assembly to the top probe pair likely distorted the local field lines, an effect that was not present for the bottom pair. Future experiments should ensure that all auxiliary assemblies are either grounded to the same reference as the gondola and positioned at a greater distance from the sensors to minimize such asymmetries. Finally, the use of a high-resolution (16-bit, 64 Hz) onboard data acquisition system proved essential, as standard telemetry was insufficient for capturing the sub-millivolt signals characteristic of the fair-weather stratospheric electrical environment.

Another BEENS experiment is planned to address the remaining shortcomings and expand the scope of the measurements from the Indian sector. These include further miniaturization to reduce balloon volume (~5000 cu. m or less) and total gondola weight to under 75 kg. Passive spin methods will target rotation rates below 1 RPM to eliminate motor interference. Use of standardized 16-bit ADCs will be prioritized to overcome the resolution limits of earlier 12-bit systems. Additionally, daytime flights with 6-8 hour float durations around sunrise and sunset will be attempted to investigate ionospheric signatures and variations in the vertical electric field. Finally, the scope will expand to include AC electric and magnetic field measurements, providing a window into plasma waves originating in the ionosphere and magnetosphere. In conclusion, the BEENS-2 experiment has provided a robust framework for low-latitude stratospheric electric field measurements, combining technical innovation with consistent scientific observations to advance our understanding of the near-space electrodynamic environment.

Data availability

The raw 1 Hz telemetry data and auxiliary altitude profiles supporting the findings of this study are openly available in Zenodo at https://doi.org/10.5281/zenodo.20201663. The high resolution (64 sps) data from onboard data acquisition system used for the primary analysis are available from the authors upon reasonable request.

Author contributions

KJ and SG conceptualized and designed the experimental framework and payload configuration. PM and CS were responsible for hardware realization. The field experiments and data collection were carried out by KJ, PM, CS, and SG. SS served as the project coordinator. TVR coordinated the balloon operations essential for the experiment. APD provided overall scientific leadership and was instrumental in securing the necessary funding and institutional support for the BEENS-2 experiment.

Competing interests

The authors declare that they have no conflict of interest.

© Author(s) 2026. CC BY 4.0 License.

Disclaimer

Copernicus Publications adds a standard disclaimer: "Copernicus Publications remains neutral with regard to jurisdictional claims made in the text, published maps, institutional affiliations, or any other geographical representation in this paper. While Copernicus Publications makes every effort to include appropriate place names, the final responsibility lies with the authors. Views expressed in the text are those of the authors and do not necessarily reflect the views of the publisher."

Acknowledgements

The authors gratefully acknowledge the staff of the TIFR Balloon Facility for their technical assistance and support in conducting the balloon operations for the BEENS-2 experiment.

Financial support

This work is supported by the Department of Science and Technology, Government of India.

References

Bering, III, E. A., Kelley, M. C., and Mozer, F. S.: Observations of an intense daytime ionospheric electric field, J. Geophys. Res., 82, 1925–1932, 1977.

D'Angelo, N., Iversen, I. B., and Madsen, M. M.: Influence of the dawn-dusk potential difference on the stratospheric electric field in the polar cap, J. Geophys. Res., 87, 8933–8940, 1982.

Fahleson, U. V.: Theory of electric field measurements conducted in the magnetosphere with electric probes, Space Sci. Rev., 7, 238–262, 1967.

Gurubaran, S., Manu, S., Jawahar, K., Emperumal, K., Mahavarkar, P., and Buduru, S. K.: A high-altitude balloon experiment to probe stratospheric electric fields from low latitudes, Ann. Geophys., 35, 189–201, 2017.

Gupta, S. P.: Importance of electric field measurement over low latitudes at stratospheric heights by balloons, Adv. Space Res., 3, 115–116, 1983.

Hays, P. B. and Roble, R. G.: A quasi-static model of global atmospheric electricity, 1. The lower atmosphere, J. Geophys. Res., 84, 3291–3305, 1979.

Holzworth, R. H.: High latitude stratospheric electrical measurements in fair and foul weather under various solar conditions, J. Atmos. Terr. Phys., 43, 1115–1125, 1981.

Holzworth, R. H.: Conductivity and electric field variations with altitude in the stratosphere, J. Geophys. Res., 96, 12857–12864, 1991.

https://doi.org/10.5194/egusphere-2026-3904
Preprint. Discussion started: 12 August 2026
© Author(s) 2026. CC BY 4.0 License.

Holzworth, R. H. and Bering, III, E. A.: Ionospheric electric fields from stratospheric balloon-borne probes, in: Measurement Techniques in Space Plasmas: Fields, edited by: Pfaff, R. F., Borovsky, J. E., and Young, D. T., AGU, Washington, DC, USA, Geophysical Monograph 103, 1998.

Holzworth, R. H., et al.: Balloon observations of temporal variation in the global circuit compared to global lightning activity, Proc. 17th ESA Symposium on European Rocket and Balloon Programmes and Related Research, Sandefjord, Norway, 2005.

Jawahar, K., Manu, S., and Gurubaran, S.: A differential electrometer for vector electric field measurements on a balloon platform, Current Sci., 111, 624–626, 2016.

Kelley, M. C.: The Earth's Ionosphere: Plasma Physics and Electrodynamics, Academic Press, San Diego, 1989.

Mahavarkar, P., et al.: Engineering and Validation of a Multi-Material, Balloon Payload for Stratospheric Electric Field Measurements, J. Instrum., submitted, 2026.

Mozer, F. S. and Serlin, R.: Magnetospheric electric field measurements with balloons, J. Geophys. Res., 74, 4739–4754, 1969.

Panneerselvam, C., et al.: Fair-weather atmospheric electricity study over South India, J. Atmos. Sol.-Terr. Phys., 69, 1681–1693, 2007.

Pasko, V. P., Stanley, M. A., Mathews, J. D., Inan, U. S., and Woods, T. G.: Electrical discharge from a thundercloud top to the lower ionosphere, Nature, 416, 152–154, 2002.

Rycroft, M. J., Israelsson, S., and Price, C.: The global atmospheric electric circuit, solar activity and climate change, J. Atmos. Sol.-Terr. Phys., 62, 1563–1576, 2000.

Sikka, D. R. and Narasimha, R.: Genesis of the tropical monsoon and the role of the Indian subcontinent, Proc. Indian Acad. Sci., 104, 157–187, 1995.

Udare, R. S., Rajaram, R., Ogawa, T., and Yashuhara, M.: Height profile of vertical electric field and conductivity over Hyderabad, Indian J. Radio Space Phys., 20, 307–309, 1991.

Williams, E. R.: The global electrical circuit: a review, Atmos. Res., 91, 140–152, 2009.